Joint Estimation of Doppler Stretch and Time Delay of Wideband Echoes for LFM Pulse Radar Based on Sigmoid-FRFT Transform under the Impulsive Noise Environment

Li Li [1,2,*], Nicolas H. Younan [2,*] and Xiaofei Shi [2,3]

[1] College of Information Engineering, Dalian University, Dalian 116622, China
[2] Department of Electrical and Computer Engineering, Mississippi State University, Starkville, MS 39762, USA
[3] Information Science and Technology College, Dalian Maritime University, Dalian 116026, China; shixiaofei@dlmu.edu.cn
[*] Correspondence: ffsimplemsu@gmail.com (L.L.); younan@ece.msstate.edu (N.H.Y.)

Abstract: To overcome the limitation of performance degradation of existing methods based on fractional Fourier transform in impulsive noise, and fractional lower-order statistics based method dependence on a priori knowledge of the noise, a novel Sigmoid fractional Fourier transform (Sigmoid-FRFT) is presented in this paper. This novel approach is then used to estimate the Doppler stretch and time delay. Furthermore, the properties of the Sigmoid transform, robustness and boundedness of the Sigmoid-FRFT to the $S\alpha S$ noise, and the computation complexity of the Sigmoid-FRFT method are presented to evaluate the performance of the proposed method. Simulation results and theoretical analysis are presented to demonstrate the applicability of the forgoing method. It is shown that the proposed method not only can effectively suppress impulsive noise interference but also does not need a priori knowledge of the noise, with higher estimation accuracy and lower computational complexity in impulsive noise environments.

Keywords: impulsive noise; Sigmoid transform; fractional Fourier transform; linear frequency modulation (LFM) pulse radar; parameter estimation

1. Introduction

In a radar or a sonar system, the received signal, in comparison with the transmitted waveform, often contains both time delay (TD) and Doppler stretch (DS). At present, this topic has attracted many researchers' attention [1,2]. Various algorithms have been proposed to estimate these parameters. For instance, Zhang et al. proposed an expectation-maximization based estimator to estimate delay and Doppler of a moving target in a passive radar [3]. Qu et al. proposed a method based on the wideband ambiguity function to estimate time delay and Doppler stretch for a wideband signal [4]. Niu et al. presented a wavelet-based wideband cross ambiguity function (WB-WBCAF) method to estimate the time delay and Doppler stretch between two received signals that are contaminated by noise [5]. Friedlander proposed an algorithm based on a computationally efficient search-free frequency estimation technique for the sum of complex exponentials for Doppler-Delay Estimation [6]. These methods may solve such parameter estimation problems in the Gaussian noise environment. However, the performance of these methods degenerates severely in the impulsive noise environment.

To suppress the impulsive noise interference, many parameter estimation algorithms based on the fractional lower-order statistics (FLOS) have been proposed [7–13]. Li et al. proposed a new method based on sparse representation of the fractional lower order statistics to estimate Direction of arrival

(DOA) in impulsive noise [7]. Ma et al. proposed the fractional lower order covariance method and least mean p norm criterion for time delay estimation (TDE), and the fractional lower order ambiguity function for joint time delay of arrival (TDOA) and frequency delay of arrival (FDOA) estimation [8]. Long et al. presented the applications of fractional lower order time frequency representation to machine bearing fault diagnosis [9].

Time-frequency distribution is a useful tool to extract helpful information of the received signal. Various time frequency distribution methods based on fractional lower order statistics have been proposed, such as short time Fourier transform based on fractional lower order statistics [10], Wigner–Ville distributions based on fractional lower order statistics [11], fractional power spectrum density based on fractional lower order statistics [12], and fractional correlation based on fractional lower-order statistic [13]. Li et al. proposed a novel method that combines the fractional lower order statistics and fractional power spectrum density (FLOS-FPSD) for suppressing the impulsive noise and estimating parameters for a bistatic multiple input and multiple output (MIMO) radar system in the impulse noise environment [12]. The fractional correlation based on fractional lower-order statistic (FLOS-FC) method has been proposed in an impulsive noise environment [13], where the Doppler stretch and time delay are jointly estimated by peak searching of the FLOS-FC. Therefore, in relevant prior publications, the FLOS theory has been always employed to suppress the impulsive noise interference.

However, the performance of these algorithms based on fractional lower order statistics may degrade seriously for an inappropriate fractional lower order moment p [14–16]. According to the fractional lower order statistics theory, the relationship between the fractional lower order moment p and characteristic exponent α must satisfy $1 \leq p < \alpha$ or $0 < p < \alpha/2$. Therefore, the methods based on fractional lower order statistics depend on a priori knowledge of the noise.

To overcome these limitations, a novel time-frequency transform, combining fractional Fourier transform and Sigmoid transform and known as Sigmoid fractional Fourier transform, is proposed to estimate the Doppler stretch (DS) and time delay (TD) of wideband echoes for linear frequency modulation (LFM) pulse radar under impulsive noise environment. This technique does not need a priori knowledge of impulsive noise.

This paper is organized as follows. Section 2 presents a signal model of wideband echoes in impulsive noise environment. In Section 3, a novel Sigmoid fractional Fourier transform (Sigmoid-FRFT) is defined. In Section 4, a novel Doppler stretch and time delay estimation method based on Sigmoid-FRFT for impulsive noise is proposed, and performance analysis of the Sigmoid-FRFT method is presented. In Section 5, the performance of the parameter estimation algorithm is studied through extensive numerical simulations. Finally, conclusions are drawn in Section 6.

2. Signal Model and Noise Model

2.1. Wideband Signal Model

The wideband signal model for constant amplitude LFM signals by L targets arriving can be described as [17]

$$y(t) = \sum_{l=1}^{L} \eta_l x(\sigma_l(t - \tau_l)) + n(t), \tag{1}$$

where η_l denotes the attenuation factor of the lth multipath, σ_l is the Doppler stretch, τ_l is the time delay, $x(t)$ denotes the transmitted LFM signal,

$$x(t) = A \exp\left(j2\pi\left(f_0 t + \frac{1}{2}\mu_0 t^2\right)\right), \tag{2}$$

which f_0 is the initial frequency, μ_0 is the modulation rate, A denotes the signal amplitude. The noise $n(t)$ is a sequence of i.i.d isotropic complex symmetric α-stable ($S\alpha S$) random variable.

2.2. SαS Distribution Noise Model

The characteristic function of the *SαS* distribution is given by [8,14],

$$\psi(\omega) = \exp\left(-\gamma|\omega|^{\alpha}\right), \tag{3}$$

where α ($0 < \alpha \le 2$) is the characteristic exponent. The characteristic exponent controls the heaviness of the tails of the density function. The tails are heavier, and thus the noise more impulsive. When $\alpha = 2$, the *SαS* distribution reduces to the Gaussian distribution. The parameter γ, usually called the dispersion, is a positive constant related to the scale of the distribution.

The signal-to-noise condition of *SαS* using the generalized signal-noise-ratio (GSNR), which is described as

$$\text{GSNR} = 10\lg\left(\sigma_x^2/\gamma\right), \tag{4}$$

where σ_x^2 is the variance of the underlying signal.

3. Sigmoid Fractional Fourier Transform

3.1. Fractional Fourier Transform

The continuous FRFT [18,19] of a signal $x(t)$ with a rotation angle β is defined as

$$X(\beta, m) = F^{\beta}[x(t)](m) = \int_{-\infty}^{+\infty} x(t)K_b(t, m)\mathrm{d}t, \tag{5}$$

where F^b denotes the FRFT operator, $b(0 < b \le 2)$ denotes the fractional order, $\beta \equiv b\pi/2$, and $K_b(t, m)$ is the kernel function of the fractional Fourier transform. $K_b(t, m)$ can be expressed as

$$K_b(t, m) = \begin{cases} A_\beta \exp\left(j\pi(t^2 \cot\beta - 2mt\csc\beta + m^2 \cot\beta)\right), & \beta \ne n\pi \\ \delta(t - m), & \beta = 2n\pi \\ \delta(t + m), & \beta = (2n+1)\pi \end{cases}, \tag{6}$$

where $A_\beta = \sqrt{1 - j\cot\beta}$ and m is the frequency in FRFT domain. When $\beta = 2n\pi + \frac{\pi}{2}$, $K_b(t, m)$ coincides with the kernel of the Fourier transform, and the FRFT reduces to the conventional Fourier transform. The kernel has the following properties: $K_b(t, m) = K_b(m, t)$ and $K_{-b}(t, m) = K_b^*(t, m)$.

3.2. FRFT of LFM Signal

From Equations (5) and (6), the FRFT of the LFM signal $x(t)$ can be expressed as

$$X(\beta, m) = A_\beta A \exp\left(j\pi m^2 \cot\beta\right) \int_{-T/2}^{T/2} \exp(j2\pi t(f_0 - m\csc\beta)) \exp\left(j\pi t^2(\cot\beta + \mu_0)\right)\mathrm{d}t. \tag{7}$$

When $\mu_0 = -\cot\beta$, $X(\beta, m)$ has the best energy-concentrated property and an optimal rotation angle β_0 exists to maximize the peak amplitude of $X(\beta, m)$. Accordingly, $b_0 = 2\beta_0/\pi$ is called the optimal fractional order. The $X(\beta_0, m)$ forms a pulse in the FRFT domain and its peak value appears at (β_0, m_0) as

$$(\beta_0 = -\text{arc}\cot\mu_0, m_0 = f_0 \sin\beta_0) = \underset{\beta, m}{\text{argmax}}|X(\beta, m)|. \tag{8}$$

According to Equation (8), we can find that the rotation angle β only depends on the frequency modulation rate μ_0.

Similarly, the FRFT of the echo signal $y(t)$ can be written as

$$
\begin{aligned}
Y(\beta, m) &= \sum_{l=1}^{L} \int_{-T/2}^{T/2} A_\beta \eta_l \exp\left(j2\pi\left(\left(\sigma_l f_0 - \mu_0 \sigma_l^2 \tau\right) t + \tfrac{1}{2}\mu_0 \sigma_l^2 t^2 \right)\right) \\
&\quad \times \exp\left(j\pi\left(t^2 \cot\beta - 2mt \csc\beta + m^2 \cot\beta \right)\right) \mathrm{d}t + N(\beta, m) \\
&= \sum_{l=1}^{L} A_\beta \eta_l \exp\left(j2\pi\left(\tfrac{1}{2}\mu_0 \sigma_l^2 \tau_l^2 - \sigma_l f_0 \tau_l + \tfrac{1}{2} m^2 \cot\beta \right)\right) \\
&\quad \times \int_{-T/2}^{T/2} \exp\left(j2\pi t \left(\sigma_l f_0 - \mu_0 \sigma_l^2 \tau - m \csc\beta\right)\right) \exp\left(j\pi t^2 \left(\mu_0 \sigma_l^2 + \cot\beta\right)\right) \mathrm{d}t + N(\beta, m)
\end{aligned}
\tag{9}
$$

where $N(\beta, m)$ denotes the FRFT of the noise $n(t)$. If and only if

$$
\begin{cases}
\sigma_l f_0 - \mu_0 \sigma_l^2 \tau = m_l \csc\beta_l \\
\cot\beta_l = -\mu_0 \sigma_l^2
\end{cases}.
\tag{10}
$$

$Y(\beta, m)$ forms L pulses in the FRFT domain and these peaks appear at (β_l, m_l). Thus, the estimation of the Doppler stretch and time delay becomes a problem of locating the peak point of $Y(\beta, m)$. Then, it follows directly from Equation (10) that the Doppler stretch and time delay are estimated by

$$
\begin{cases}
\hat{\sigma}_l = \sqrt{-\dfrac{\cot\beta_l}{\mu_0}} \\
\hat{\tau}_l = \dfrac{\hat{\sigma}_l f_0 - m_l \csc\beta_l}{\mu_0 \hat{\sigma}_l^2}
\end{cases}.
\tag{11}
$$

3.3. Sigmoid Transform

Sigmoid is a commonly used nonlinear transformation [20–22]. Its definition can be shown as

$$
\mathrm{Sigmoid}[x(t)] = \frac{2}{1 + \exp[-x(t)]} - 1.
\tag{12}
$$

For a $S\alpha S$ process with $a = 0$, the Sigmoid transform has the following properties.

Property 1: If $x(t)$ is a $S\alpha S$ process with $\beta = 0$ and $a = 0$, then $\mathrm{Sigmoid}[x(t)]$ is a symmetric distribution with zero mean in its probability density function, and has the finite second order moment with zero mean (referred as a second order moment process).

Property 2: $\mathrm{Sigmoid}[x(t)]$ has the same frequency shift as $x(t)$.

Property 3: $\mathrm{Sigmoid}[x(t)]$ has the same time delay as $x(t)$.

Since Properties 1 and Properties 2,3 have been proved in [4] and [15], respectively, the relevant proof will be skipped.

3.4. Definition of the Sigmoid-FRFT

To overcome the limitations that the performance degradation of the existing methods based on fractional Fourier transform in the impulsive noise and the fractional lower-order statistics-based methods dependencies on the priori knowledge of the noise, this paper proposes a novel Sigmoid fractional Fourier transform (Sigmoid-FRFT), combining the fractional Fourier transform and the Sigmoid transform. The definition of the Sigmoid-FRFT $X_{\mathrm{Sigmoid}}(\beta, m)$ is expressed as

$$
X_{\mathrm{Sigmoid}}(\beta, m) = F_{\mathrm{Sigmoid}}^b[x(t)](m) = \int_{-\infty}^{+\infty} Sigmoid[x(t)] \, K_\beta(t, m) \mathrm{d}t.
\tag{13}
$$

Since the FRFT spectrum $X(\beta, m)$ of the LFM signal $x(t)$ has the energy-concentrated property, the Sigmoid-FRFT spectrum $X_{\mathrm{Sigmoid}}(\beta, m)$ of $\mathrm{Sigmoid}[x(t)]$ demonstrates the same property according to properties of the Sigmoid transform. Furthermore, $X(\beta, m)$ and $X_{\mathrm{Sigmoid}}(\beta, m)$ form the pulse at the same location in the FRFT domain.

Equation (13) is the definition of the Sigmoid-FRFT that is used throughout this paper. Searching for the peaks of the Sigmoid-FRFT $X_{\text{Sigmoid}}(\beta, m)$, the $X_{\text{Sigmoid}}(\beta, m)$ forms a pulse in the FRFT domain and its peak value appears at (β_0, m_0) as

$$\left(\beta_0 = -\operatorname{arc\,cot} \mu_0, m_0 = f_0 \sin \beta_0\right) = \underset{\beta, m}{\operatorname{argmax}} \left| X_{\text{Sigmoid}}(\beta, m) \right|. \tag{14}$$

Figure 1 shows the performance of suppressing the impulsive noise FRFT and the Sigmoid-FRFT under an impulsive noise with GSNR = 5 dB with $\alpha = 1.2$. Figure 1a,c represents the time-frequency distribution of the FRFT and the Sigmoid-FRFT of the impulsive noise. Figure 1b,d represents the time-frequency distribution of the FRFT and the Sigmoid-FRFT of the LFM signal with impulsive noise. From Figure 1, it is clearly seen that identifying the correct peak location is not trivial as the FRFT peak cannot be distinguished from the impulsive noise. Accordingly, the estimation performance of the FRFT method degrades severely in the impulsive noise environment. After the application of the Sigmoid transformation, the impulsive noise is suppressed effectively and the Sigmoid-FRFT spectrum forms an obvious pulse in the FRFT domain. Thus, the method based on the Sigmoid-FRFT yields better estimation performance.
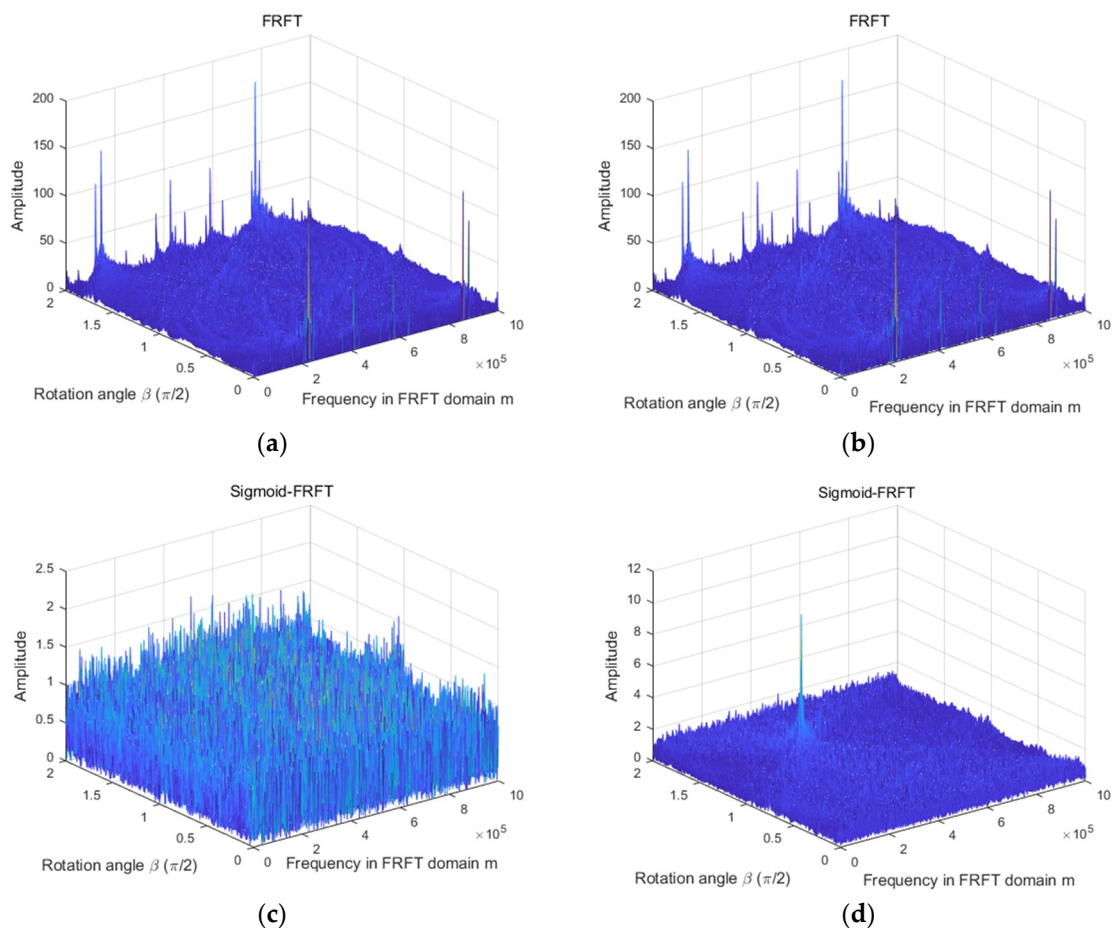

Figure 1. Time-frequency distribution of the fractional Fourier transform (FRFT) and Sigmoid-FRFT in an impulsive noise environment. (**a**) FRFT of the impulsive noise; (**b**) FRFT of the linear frequency modulation (LFM) signal with impulsive noise; (**c**) Sigmoid-FRFT of the impulsive noise; (**d**) Sigmoid-FRFT of the LFM signal with impulsive noise.

4. Parameter Estimation Based on Sigmoid Fractional Fourier Transform (Sigmoid-FRFT)

4.1. Estimation of Doppler Stretch and Time Delay based on Sigmoid-FRFT

According to Equation (13), we can obtain the Sigmoid-FRFT $Y_{\text{Sigmoid}}(\beta, m)$ of $y(t)$ as

$$
\begin{aligned}
Y_{\text{Sigmoid}}(\beta, m) &= F^b_{\text{Sigmoid}}[y(t)](m) \\
&= F^b_{\text{Sigmoid}}\left[\sum_{l=1}^{L} \eta_l x(\sigma_l(t - \tau_l))\right](m) + F^b_{\text{Sigmoid}}[n(t)](m) \\
&= \int_{-\infty}^{+\infty} Sigmoid\left[\sum_{l=1}^{L} \eta_l x(\sigma_l(t - \tau_l))\right] K_\beta(t, m)\mathrm{d}t + N_{\text{Sigmoid}}(\beta, m)
\end{aligned}
\tag{15}
$$

where $N_{\text{Sigmoid}}(\beta, m)$ denotes the Sigmoid-FRFT of the noise $n(t)$.

Similarly, in searching for the peaks of $Y_{\text{Sigmoid}}(\beta, m)$, the Doppler stretch and time delay can be jointly estimated by

$$
\begin{cases}
\hat{\sigma}_l = \sqrt{-\dfrac{\cot \beta_l}{\mu_0}} \\
\hat{\tau}_l = \dfrac{\hat{\sigma}_l f_0 - m_l \csc \beta_l}{\mu_0 \hat{\sigma}_l^2} \\
(\beta_l, m_l) = \underset{\beta, m}{\operatorname{argmax}} \left| Y_{\text{Sigmoid}}(\beta, m) \right|
\end{cases}
\tag{16}
$$

4.2. Boundedness of Sigmoid-FRFT to the SαS Noise

Assumed the signal $x(t)$ contains the impulsive noise, we can define as

$$
x(t) = s(t) + n(t),
\tag{17}
$$

where $s(t)$ is the signal and $n(t)$ is the *SαS* random variable noise.

The fractional power spectrum function is defined as [23]

$$
P^\beta_{xx}(m) = \lim_{T \to \infty} \frac{E\left| X_{\text{Sigmoid}}(\beta, m) \right|^2}{2T},
\tag{18}
$$

where $X_{\text{Sigmoid}}(\beta, m)$ is the Sigmoid-FRFT of the signal $x(t)$. Then, substituting Equation (13) into Equation (18), we get

$$
\begin{aligned}
P^\beta_{xx}(m) &= \lim_{T \to \infty} \frac{1}{2T} E\left[\int_{-T}^{+T} Sigmoid[x(t_1)] K_\beta(t_1, m)\mathrm{d}t_1 \int_{-T}^{+T} Sigmoid^*[x(t_2)] K^*_\beta(t_2, m)\mathrm{d}t_2\right] \\
&= \lim_{T \to \infty} \frac{1}{2T} E\left[\int_{-T}^{+T} \int_{-T}^{+T} K_\beta(t_1, m) K^*_\beta(t_2, m) Sigmoid^*[x(t_2)] Sigmoid[x(t_1)]\,\mathrm{d}t_1 \mathrm{d}t_2\right] \\
&= \lim_{T \to \infty} \frac{1}{2T} \int_{-T}^{+T} \int_{-T}^{+T} K_\beta(t_1, m) K^*_\beta(t_2, m) E[Sigmoid[x(t_1)] Sigmoid^*[x(t_2)]]\mathrm{d}t_1 \mathrm{d}t_2
\end{aligned}
\tag{19}
$$

where $x(t_1)$ and $x(t_2)$ are the sample values of $x(t)$.

According to the properties of the Sigmoid transform, we can obtain that $E[Sigmoid[x(t_1)] Sigmoid^*[x(t_2)]]$ is bounded for the *SαS* process because it is only involved with $Sigmoid[x(t)]$. Therefore, the boundedness of the $Sigmoid[x(t)]$ can guarantee the boundedness of $P^\beta_{xx}(m)$ under the *SαS* noise, resulting in that $X_{\text{Sigmoid}}(\beta, m)$ is bounded.

4.3. Robustness of Sigmoid-FRFT to the SαS Noise

The characteristic exponent α is used to control the thickness of the tail in the alpha stable distribution. The smaller α is, the stronger the impulsiveness is. The stronger impulsive noise has negative impacts on the estimation performance of the algorithm [24]. The FLOS theory has certain

ability to suppress impulsive noise. The suppression ability increases as the fractional lower-order moment p decreases. However, the suppression ability of the FLOS is not effective, due to $|x_1(t)|^{\langle p \rangle} > |x_2(t)|^{\langle p \rangle} > 1$ for $|x_1(t)| > |x_2(t)| > 1$. Therefore, a stronger impulsive noise cannot be suppressed effectively when the impulsiveness is extremely intense, and the estimation performance would be affected. Compared with the FLOS, for any stronger impulsive noise, the Sigmoid function can be written as

$$|\text{Sigmoid}[x(t)]| = \left| \frac{2}{1 + \exp[-x(t)]} - 1 \right| < 1. \tag{20}$$

For any $|x(t)| > 1$, we get

$$|\text{Sigmoid}[x(t)]| < 1 < |x_2(t)|^{\langle p \rangle} < |x_1(t)|^{\langle p \rangle}. \tag{21}$$

This shows that the Sigmoid transform can suppress impulsive noise better than the FLOS. Therefore, the performance of the Sigmoid transform outweighs those of the FLOS theory. The simulation results are shown in Figure 2.
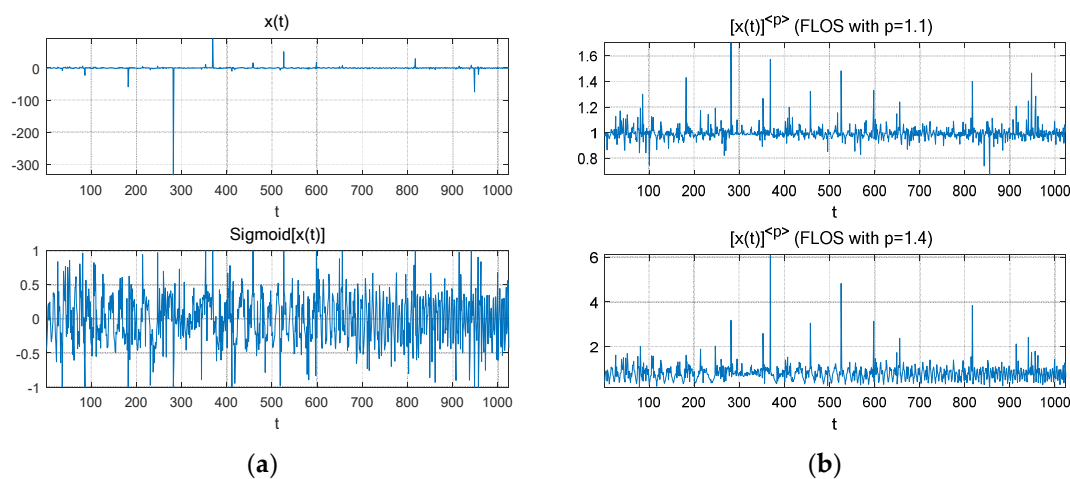

Figure 2. Comparison of the noise suppression ability for $S\alpha S$ with generalized signal-noise-ratio (GSNR) = 5 dB and α = 1.2. (**a**) Sigmoid transform; (**b**) fractional lower-order statistics (FLOS) theory.

Figure 2 shows a comparison of the impulsive noise suppression ability between two theoretical algorithms. From Figure 2, we can find that both algorithms have suppression ability of the impulsive noise, however, the performance of the Sigmoid transform method is superior to that of the FLOS. Furthermore, it is worth noting that the suppression capacity of the FLOS method is affected by the fractional lower-order moment p, where the suppression capacity of the FLOS with $p = 1.1$ outperforms that of the FLOS with $p = 1.4$.

4.4. Complexity Analysis

In this section, we evaluate the computational complexity of the proposed method, FRFT method, and FLOS-FPSD method. Suppose that the data length is N, the computational complexity of the FRFT method is $O(N \log_2 N)$ [25]. The parameter estimation based on the FLOS-FPSD method is a two step process. The first step computes the fractional lower order correlation and the second step carries the FRFT transformation. Accordingly, the computational complexity of the FLOS-FPSD algorithm is $O(N^2 + N \log_2 N)$. The proposed method based on the Sigmoid-FRFT also requires two steps. The first step performs the Sigmoid transform and the second step carries the FRFT transform. Thus, the computational complexity of the Sigmoid-FRFT algorithm is $O(N + N \log_2 N)$. Through

the computational complexity analysis, the Sigmoid-FRFT method can suppress impulsive noise interference and has a lower computational complexity compared with the FLOS-FPSD method.

5. Simulation Results

In this section, we perform three types of simulation experiments to evaluate the relative performance of the FRFT, the FLOS-FC, the FLOS-FPSD, and the Sigmoid-FRFT methods under impulsive noise, respectively.

The parameters of the transmitted LFM signal in the simulation are assumed as follows. The initial frequency $f_0 = 0.2 f_s$ and the modulation rate is set to $\mu_0 = 0.1 f_s^2 / N$. The sampling rate is set to $f_s = 1$ MHz with a sampling length of $N = 1000$. The number of multipath is $L = 2$ and the Doppler stretch and time delay are set to $\sigma_1 = 0.8$, $\sigma_2 = 1.2$, $\tau_1 = 20/f_s$ and $\tau_2 = 40/f_s$, respectively. The Root Mean Square Error (RMSE) is defined as

$$\text{RMSE} = \frac{1}{2}\left(\sqrt{\frac{1}{K}\sum_{k=1}^{K}[\hat{x}_1(k) - x_1]^2} + \sqrt{\frac{1}{K}\sum_{k=1}^{K}[\hat{x}_2(k) - \hat{x}_2]^2}\right), \tag{22}$$

where $\hat{x}_1$ and $\hat{x}_2$ are the estimation of x_1 and x_2, and K is the number of Monte Carlo. For each simulation, the number of Monte Carlo runs is 500.

5.1. Simulation 1: FRFT, FLOS-FC, FLOS-FPSD, and Sigmoid-FRFT for a Single Estimation for Two Targets

Figure 3 shows the estimation results of the FRFT, FLOS-FC, FLOS-FPSD, and Sigmoid-FRFT for a single trial of data, two targets, under impulsive noise with GSNR = 5 dB and α = 1.2. From Figure 3a,b, we can find that the FRFT algorithm fails when an impulsive occurs, where the correct peak cannot be obtained and the estimation performance degrades severely in the impulsive noise environment. The reason is that the FRFT method does not have the ability to suppress impulsive noise. The peak of the FRFT is submerged in noise.

As shown in Figure 3c, the spectrum of the FLOS-FC does not have the energy-concentrated property at a specific rotation angle. The accurate rotation angle cannot be obtained. Therefore, the FLOS-FC method fails in this noise environment. The spectrum of the FLOS-FPSD is shown in Figure 3d, and we can find that the FLOS-FPSD algorithm also fails in the impulsive noise environment because the peak of the FLOS-FPSD cannot be easily separated from the impulsive noise in the FLOS-FPSD spectrum of the echo signal with impulsive noise. The FLOS-FPSD algorithm, combining the fractional lower-order statistics theory with the fractional power spectrum density function, can effectively suppress the Alpha-stable noise interference under certain impulsive noise environments. However, when impulsiveness is stronger or GSNR is lower, the FLOS-FPSD method fails. As shown in Figure 3c,d, the FLOS-FPSD algorithm fails in the impulsive noise environment with GSNR = 5 dB and α = 1.2 because the correct peak of the FLOS-FPSD cannot be obtained. On the other hand, the Sigmoid-FRFT spectrum of the echo signal with impulsive noise forms the obvious pulse, that is because the Sigmoid transform can restrain impulsive noise interference, as illustrated in Figure 3e. Compared with the FRFT of the echo signal with no noise, it is clearly seen that the results obtained from the Sigmoid-FRFT of the echo signal with impulsive noise matches quite well and with peaks at the same location. As analyzed in Section 4.3, the Sigmoid transform can suppress impulsive noise better than the FLOS. Therefore, the proposed method based on the Sigmoid-FRFT can effectively suppress impulsive noise interference, yields an accurate peak estimation and has a better estimation performance.
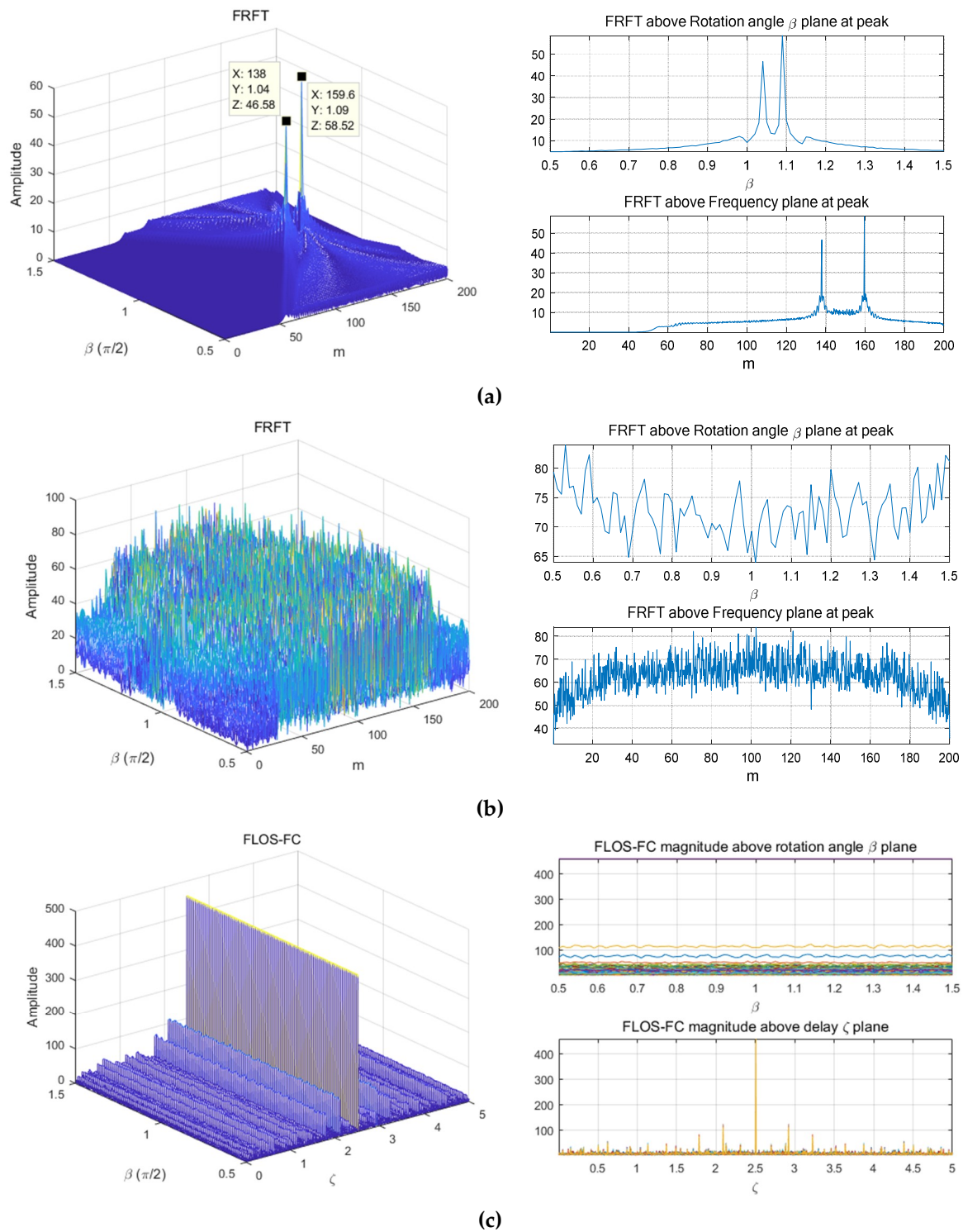
(a)

(b)

(c)

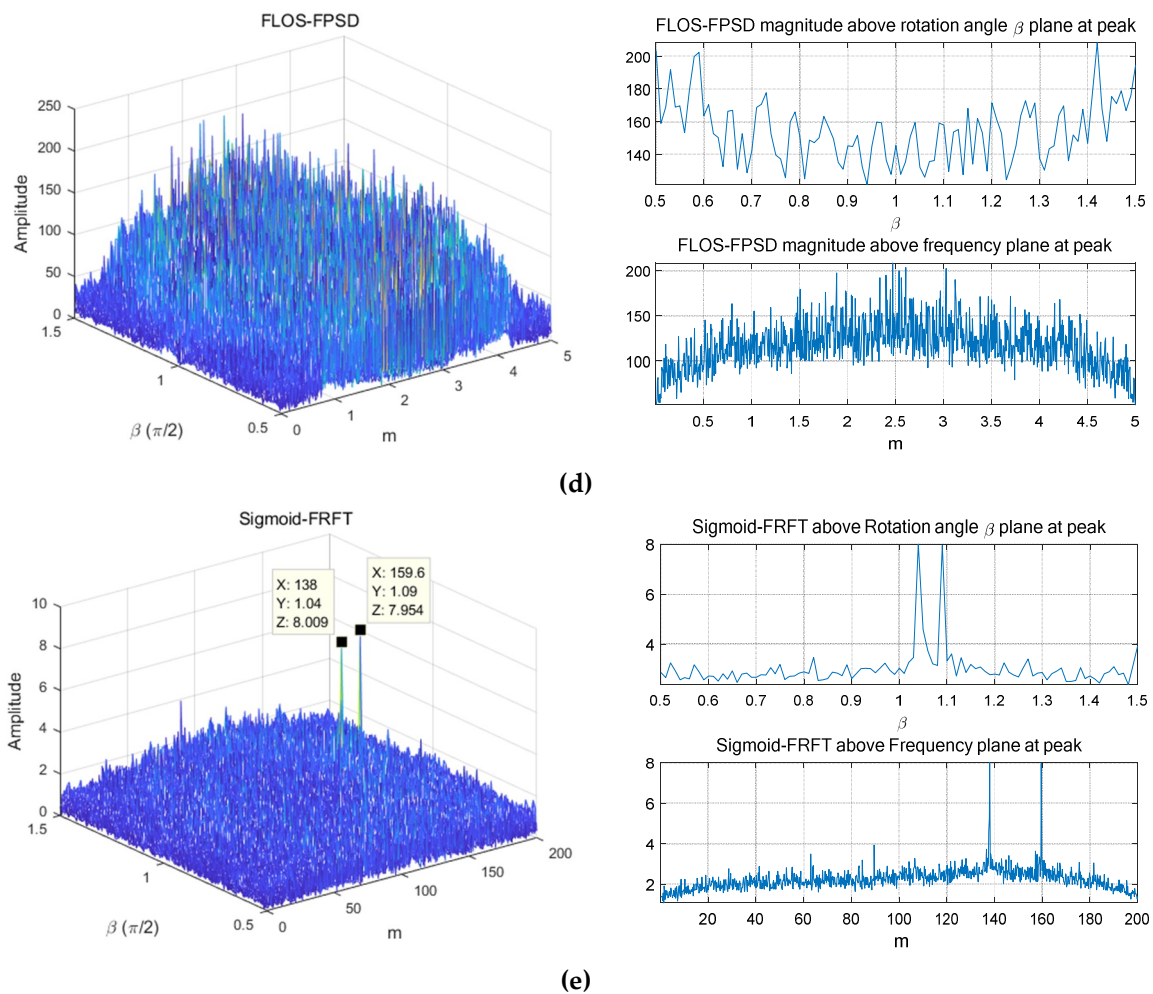**Figure 3.** *Cont.*

(d)

(e)

Figure 3. The spectrum of FRFT, the fractional correlation based on fractional lower-order statistic (FLOS-FC), the fractional lower order statistics and fractional power spectrum density (FLOS-FPSD) and Sigmoid-FRFT with impulsive noise (GSNR = 5 dB and α = 1.2). (**a**) The FRFT spectrum of the echo signal without noise and its rotation angle and frequency section planes; (**b**) the FRFT spectrum of the echo signal with impulsive noise and its rotation angle and frequency section planes; (**c**) the FLOS-FC spectrum of the echo signal with impulsive noise and its rotation angle and delay section planes; (**d**) the FLOS-FPSD spectrum of the echo signal with impulsive noise and its rotation angle and frequency section planes; (**e**) the Sigmoid-FRFT spectrum of the echo signal with impulsive noise and its rotation angle frequency section planes.

5.2. Simulation 2: Estimation Accuracy with Respect to GSNR

To evaluate the performance of TD and DS in this simulation, the characteristic exponent α is set to α = 1.2 and the fractional lower order moment p is set to $p = 1.1$ and $p = 1.5$ for the FLOS-FPSD method, respectively. The resulting RMSE performance versus GSNR is illustrated in Figure 4.

From Figure 4, we can find that the FRFT method has a poor estimation performance with impulsive noise interference. The FLOS-FPSD method on the other hand, combining the fractional lower order statistics theory with the fractional power spectrum density, can effectively suppress the Alpha-stable noise interference. Accordingly, the FLOS-FPSD method yields a clear peak under an impulsive noise. However, the performance is affected by the fractional lower-order moment p value. According to the fractional lower order statistics theory, the characteristic exponent of the noise must be estimated to ensure $1 \leq p < \alpha$ or $0 < p < \alpha/2$. The methods employing the FLOS theory cannot accurately estimate the parameters if there is no a priori knowledge of the characteristic exponent. On

the contrary, the Sigmoid-FRFT has clear peaks because the Sigmoid-FRFT cannot be affected by the fractional lower-order moment p. Therefore, we can accurately obtain the peaks of the Sigmoid-FRFT in impulsive noise environment.
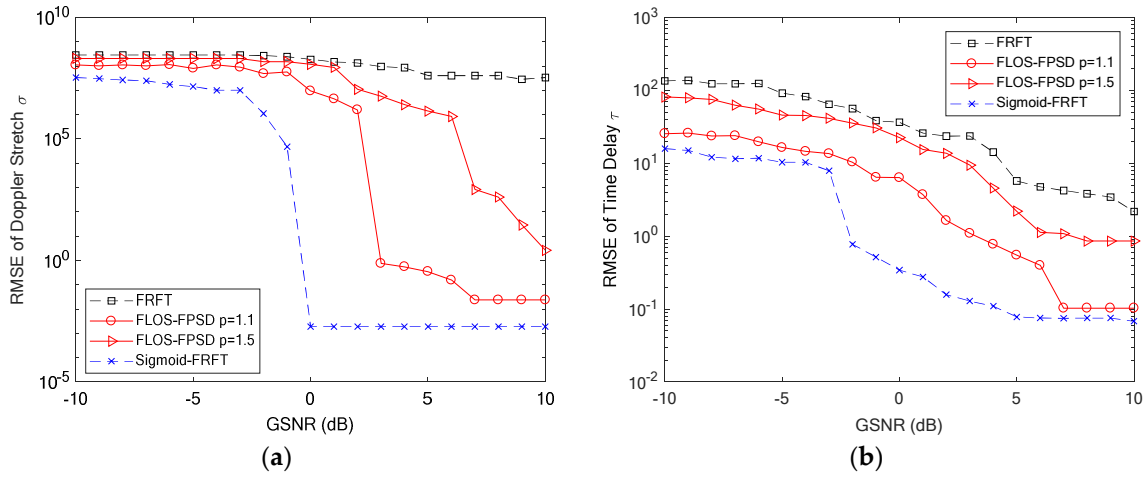

Figure 4. Root Mean Square Error (RMSE) of parameters versus GSNR. (**a**) Doppler stretch; (**b**) time delay.

5.3. Simulation 3: Estimation Accuracy with Respect to Characteristic Exponent α

To measure the estimation performance of TD and DS, the fractional lower order moment p is set to $p = 1.1$ and $p = 1.5$ for the FLOS-FPSD method, respectively. The GSNR is set to GSNR = 5 dB. Figure 5 shows the performance versus characteristic exponent α. From Figure 5, we can find that the FRFT algorithm has a better estimation performance when the characteristic exponent α is close to 2. The FLOS-FPSD method may suppress impulsive noise interference employing the fractional lower order statistic theory. The performance of the FLOS-FPSD method is shown to be better than that of the FRFT method.
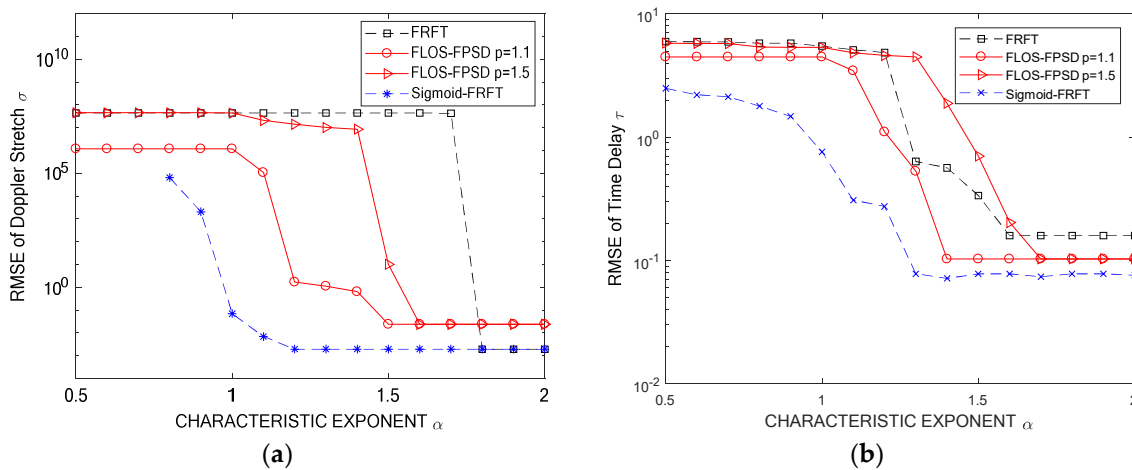

Figure 5. RMSE of parameters versus Characteristic Exponent α. (**a**) RMSE of Doppler stretch; (**b**) RMSE of time delay.

Since the suppression impulsive noise performance of the Sigmoid transform outweighs that of the FLOS theory, the estimation performance of the Sigmoid-FRFT algorithm is superior to that of the FLOS-FPSD algorithm.

6. Conclusions

In this paper, a novel time-frequency transform, Sigmoid fractional Fourier transform, is proposed. The expression of the Sigmoid-FRFT is defined and the properties of the Sigmoid transform is presented. Next, the method based on the Sigmoid-FRFT is developed to estimate the Doppler stretch and time delay of wideband echoes for an LFM pulse radar under impulsive noise environment. Furthermore, boundedness and robustness of the Sigmoid-FRFT to $S\alpha S$ noise, and computation complexity of the Sigmoid-FRFT are presented to evaluate the performance of the proposed method. Simulation results and theory analysis are presented to illustrate the validity of the foregoing method. It is clearly shown that the proposed method not only can effectively restrain impulsive noise interference but also does not depend on a priori knowledge of noise and yields a higher estimation accuracy and lower computational complexity in an impulsive noise environment.

Author Contributions: All the authors made significant contributions to this work. L.L. proposed the approach, prepared experimental data, and analyzed experimental results; N.H.Y. supervised the main idea, provided advice for the preparation and revision of the work; X.S. performed the experiments and revised the paper.

Conflicts of Interest: The authors declare no conflict of interest

References

1. Geroleo, F.; Brandt-Pearce, M. Detection and estimation of LFMCW radar signals. *IEEE Trans. Aerosp. Electron. Syst.* **2012**, *48*, 405–418. [CrossRef]
2. Govoni, M.; Li, H.; Kosinski, J. Low probability of interception of an advanced noise radar wavefor m with linear-FM. *IEEE Trans. Aerosp. Electron. Syst.* **2013**, *49*, 1351–1356.
3. Zhang, X.; Li, H.; Liu, J.; Himed, B. Joint delay and Doppler estimation for passive sensing with direct-path interference. *IEEE Trans. Signal Process.* **2016**, *64*, 630–640. [CrossRef]
4. Qiu, T.; Wang, H.; Zhang, Y.; Bao, H. Non-linear transform-based robust adaptive latency change estimation of evoked potentials. *Methods Arch.* **2002**, *41*, 331–336.
5. Niu, X.; Ching, P.; Chan, Y. Wavelet based approach for joint time delay and Doppler stretch measurements. *IEEE Trans. Aerosp. Electron. Syst.* **1999**, *35*, 1111–1119. [CrossRef]
6. Zhao, Y.; Yu, H.; Wei, G.; Ji, F.; Chen, F. Parameter estimation of wideband underwater acoustic multipath channels based on fractional Fourier transform. *IEEE Trans. Signal Process.* **2016**, *64*, 5396–5408. [CrossRef]
7. Li, S.; He, R.; Lin, B.; Sun, F. DOA estimation based on sparse representation of the fractional lower order statistics in impulsive noise. *IEEE CAA J. Autom. Sin.* **2018**, *5*, 860–868. [CrossRef]
8. Ma, X.; Nikias, C. Joint estimation of time delay and frequency delay in impulsive noise using fractional lower order statistics. *IEEE Trans. Signal Process.* **1996**, *44*, 2669–2687.
9. Long, J.; Wang, H.; Li, P.; Fan, H. Applications of fractional lower order time frequency representation to machine bearing fault diagnosis. *IEEE CCA J. Autom. Sin.* **2017**, *4*, 734–750. [CrossRef]
10. Al-Manie, M.A.; Wang, J.W. Time-frequency analysis by evolutionary periodogram with application in gear fault diagnosis. *Int. J. Wavelets Multiresolut. Inf. Process.* **2010**, *8*, 679–693. [CrossRef]
11. Dong, G.; Chen, J. Noise resistant time frequency analysis and application in fault diagnosis of rolling element bearings. *Mech. Syst. Signal Process.* **2002**, *33*, 212–236. [CrossRef]
12. Li, L.; Qiu, T.S. Parameter estimation based on fractional power spectrum under alpha-stable distribution noise environment in wideband bistatic MIMO radar system. *AEU Int. J. Electron. Commun.* **2013**, *67*, 947–954. [CrossRef]
13. Li, L.; Qiu, T. Parameter estimation based on fractional lower order statistics and fractional correlation in wideband bistatic MIMO radar system. *J. Commun.* **2014**, *9*, 745–750. [CrossRef]
14. Gonzalez, J.; Griffith, D.; Arce, G. Zero-order statistics: A mathematical framework for the characterization of very impulsive signal. *IEEE Trans. Signal Process.* **2006**, *54*, 3839–3851. [CrossRef]
15. Li, L.; Younan, N.; Shi, X. A novel parameter estimation method based on a tuneable Sigmoid in alpha-stable distribution noise environments. *Sensors* **2018**, *18*, 3012. [CrossRef] [PubMed]

16. Li, L.; Qiu, T. A novel phase parameter estimation method of quadratic FM signal based on Sigmoid fractional ambiguity function in impulsive noise environment. *AEU Int. J. Electron. Commun.* **2018**, *93*, 268–276. [CrossRef]

17. Chen, R.; Wang, Y. Efficient detection of chirp signals based on the fourth-order original moment of fractional spectrum. *Circ. Syst. Signal Process.* **2014**, *33*, 1585–1596. [CrossRef]

18. Kang, X.; Tao, R.; Zhang, F. Multiple-parameter discrete fractional transform and its applications. *IEEE Trans. Signal Process.* **2016**, *64*, 3402–3417. [CrossRef]

19. Zhang, F.; Tao, R. Power spectral estimation and its application in fractional Fourier domain. *Acta Electron. Sin.* **2008**, *36*, 1723–1727.

20. Brodersen, K.H.; Daunizeau, J.; Mathys, C.; Chumbley, J.R.; Buhmann, J.M.; Stephan, K.E. Variational Bayesian mixed-effects inference for classification studies. *Neuroimage* **2013**, *76*, 345–361. [CrossRef]

21. Saini, N.; Sinha, A. Face and palmprint multimodal biometric systems using Gabor–Wigner transform as feature extraction. *Pattern Anal. Appl.* **2015**, *18*, 921–932. [CrossRef]

22. Lang, H.; Zhang, J.; Zhang, X.; Meng, J. Ship classification in SAR Image by joint feature and classifier selection. *IEEE Geosci. Remote Sens. Lett.* **2016**, *13*, 212–216. [CrossRef]

23. Tao, R.; Zhang, F.; Wang, Y. Fractional power spectrum. *IEEE Trans. Signal Process.* **2008**, *56*, 4199–4206.

24. Yu, L.; Qiu, T.S.; Luan, S.Y. Robust joint estimation for time delay and Doppler frequency shift based on generalized sigmoid cyclic cross-ambiguity function. *IET Radar Sonar Navig.* **2017**, *11*, 721–728.

25. Tao, R.; Deng, B.; Wang, Y. Research of fractional Fourier transform in signal processing. *SCI China Ser. E* **2006**, *36*, 113–136. [CrossRef]